sCO2-4-NPP: Innovative sCO2-Based Heat Removal Technology for an Increased Level of Safety of Nuclear Power Plants

Deliverable 4.1

Test results of the improved small-scale turbomachine

Work programme topic addressed: NFRP-2018-10: Encouraging innovation in nuclear safety for the benefit of European citizen

Type of action: Innovation action

Grant Agreement number:	847606
Start date of project: 1 September 2019	Duration: 36 months
Lead beneficiary of this deliverable:	UDE
Due date of deliverable: 18/02/2021	Actual submission date: 22/07/2022
	Version #: R1.0

Type		
R	Document, report excluding the periodic and final reports	X
DEM	Demonstrator, pilot, prototype, plan designs	
DEC	Websites, patents filing, press & media actions, videos, etc.	
OTHER	Software, technical diagram, etc.	
Dissemination level		
PU	PUBLIC, fully open, e.g. web	X
CO	CONFIDENTIAL, restricted under conditions set out in Model Grant Agreement	

Revision History

Release	Date	Reason for Change	Author	Distribution
R0.1	18/05/2021	First draft	Hacks	All partners
R0.4	17/06/2021	Second draft	Hacks	All partners
R1.0	22/07/2022	Final	Hacks	Consortium & EC services

Deliverable Contributors

Authors

Partner	Name
UDE	Alexander Hacks

Contributors

Partner	Name
TU Kaiserslautern (subcontractor – aerostatic gas bearings)	Artur Schimpf

Internal Reviewers

Partner	Name
GfS	Frieder Hecker
UDE	Sebastian Schuster
UDE	Dieter Brillert

Table of contents

1 List of Acronyms 5
2 Executive Summary 6
3 Introduction 7
4 Improvement of the sCO2-HeRo turbomachine 9
4.1 Summary of reasons and expected effects of the turbomachine improvement 9
4.2 Overview on new turbomachine design 9
5 Operation of improved turbomachine 11
5.1 Operation of magnetic bearings 11
5.2 Improved measurements 12
5.3 Improved cycle design 13
5.4 Start and Stop procedures 13
5.4.1 Start procedure 14
5.4.2 Stop procedure 16
6 Mitigation – Aerostatic gas bearings 17
6.1 Overview of aerostatic gas bearings 17
6.2 Results aerostatic gas bearings 19
7 Conclusion 22
8 References 23
Appendix A Piping and Instrumentation Diagram 24
Appendix B Pictures of improved turbomachine 26

List of Tables

Table 1: Change of rotor dimensions for application of magnetic bearings 10

List of Figures

Figure 1: 3D-printed 1:1 scale models of TACs developed in the sCO2-HeRo project (left) and their improved version from the sCO2-4-NPP project (right) for laboratory-scale experiments [8] 10
Figure 2: Leakage reduction due to lower pressure ratio by dispensing with additional compressor 12
Figure 3: Comparison of the pressure ratio versus mass flow at the impeller inlet of the improved TAC's compressor with previous measurements from the sCO2-HeRo project and CFD predictions 13

Figure 4: Operating conditions during start-up (heating up), TAC operation and shutdown (cooling down) - example from February 25, 2021 ..... *14*
Figure 5: Full Darcy Plus model *17*
Figure 6: Concept of the aerostatic gas bearing test rig *18*
Figure 7: Aerostatic bearings with porous sleeves *18*
Figure 8: Aerostatic gas bearing - bearing housing (top left), seals (top right) and test rig during initial air commissioning tests (bottom) *19*
Figure 9: Prediction of the load caring capacity at 8000 rpm *20*
Figure 10: Pressure distribution in a porous sleeve *20*
Figure 11: Validation numerical results with measurements by Mokhtar et al. [13] *21*
Figure 12: P&ID of the sCO2-HeRo cycle adopted for the improved turbomachine with magnetic bearings *25*
Figure 13: Improved TAC fully assembled during commissioning tests with air (left) and integrated in the sCO2-HeRo cycle (right) *26*

1 List of Acronyms

Abbreviation / Acronym	Description / meaning
AMB	Active magnetic bearings
CFD	Computational Fluid Dynamics
CHX	Compact heat exchanger
NPP	Nuclear power plant
P&ID	Piping and instrumentation diagram
PP	Piston pump
sCO_2	Carbon dioxide in the supercritical state
SEH	Slave electrical heater
TAC	Turbomachine of integral design with turbine, alternator and compressor in one casing
TRL	Technology readiness level
UHS	Ultimate heatsink (air cooler with fans adjustable in rotational speed)

2 Executive Summary

The goal of the sCO2-4-NPP project is to develop a robust heat removal system for a nuclear power plant with technology readiness level (TRL) 5, based on the results of the sCO2-HeRo project, in which a down-scaled heat removal system with TRL 3-4 was developed, built and tested. The task of this project is to scale the sCO2-HeRo system and components for use in a real nuclear power plant (NPP). This report focuses on the experimental validation of the technology for the turbomachinery, consisting of turbine, generator, and compressor (TAC). With the operational experience from the sCO2-HeRo project, the main improvement has been made to the rotor bearing by magnetic bearings. In addition, recommendations for the design of the TAC and the operation of the supercritical CO_2 (sCO_2) cycle have been formulated for the real NPP.

Ball bearings with conventional oil-based grease lubrication were used in the original TAC of the sCO2-HeRo project, which did not allow the system to achieve the desired robustness. The bearings were identified in the experiments as a key component/technology to be improved in the new design. Since sCO_2 extracts the oil phase from the grease, it can only be used at conditions below the critical pressure of 74 bar. This requires an additional pump to return the leakage to the main circuit to prevent loss of the CO_2. This additional component with valves, etc., reduces the robustness of the system, especially due to the risk of pump failure, which would result in the failure of the entire system. The improved design has active magnetic bearings (AMB) that perform their function in a sCO_2 environment (CO_2 in supercritical conditions).

Experiments with the magnetic bearings show significant forces acting on the rotor that must be kept in balance. The cavities in the TAC filled with sCO_2 provide an interaction between the high-density CO_2 and the rotor, resulting in forces on the shaft. This requires an appropriate rotor dynamic concept and control system to account for it. The rotor dynamic model as a basis for the control reproduces the real behavior to a very good extent, so that the experiments allow successful operation of the improved TAC. The adjustment of controller parameters (e.g. stiffness) allow the rotor to run smoothly. Thus, the experimental results validated the modeling of the AMB system in the machine, allowing a successful implementation of this technology. Furthermore, the aerodynamic design tools could be improved by new measurements of the compressor map. For risk mitigation, a feasibility study on the use of aerostatic gas bearings is carried out in addition to magnetic bearings.

Conclusion: The deliverable describes the successful implementation of a bearing technology, provides data for the validation of mechanical and aerodynamic design tools for Task 4.2 and thus completely fulfills the objective of the project.

3 Introduction

The task of this project is to scale up the sCO2-HeRo system and components, especially the TAC, for use in a nuclear power plant (NPP). The TAC for the NPP will be designed in Task 4.2, for which the deliverable will provide the necessary input regarding appropriate technology as well as design and operating strategies. The special feature of the design is a compact machine in whose machine housing CO_2 is present in a supercritical state. The proper operation of the TAC under these conditions is thus the basis for the heat removal system in NPPs.

In this deliverable, the modifications to the original TAC from the sCO2-HeRo project are described. The focus is on the bearings of the TAC and the improved design with AMBs. The integral design of the TAC, whose general advantage is the hermetic housing with no outgoing shaft, is maintained because it avoids leakage to the environment and constant refilling of the circuit with CO_2. However, in the improved TAC, the bearings operate in sCO_2. This is unusual since both the bearings of the original TAC from the sCO2-HeRo project [1] and the bearings of other turbomachinery for sCO_2 studied by research institutes and industry around the globe [2–4] operate in subcritical, gaseous CO_2. This requirement of subcritical gaseous CO_2 means that the pressure within the machine must be reduced below the inlet pressure of the compressor using an additional pump. To protect the bearings, a safety valve would open if the pump failed, resulting in a loss of CO_2 in the circuit. This poses a risk to the operation of the system and significantly reduces the robustness of the system. This additional pump is eliminated when the bearings are operated in sCO_2. With this deliverable, Task 4.1 establishes the technological basis for implementing the AMBs to operate the entire rotor in sCO_2.

The deliverable documents the operation of these bearings. The experiments show that the improved TAC can be operated with AMBs, although the control concept must be adapted. While the sCO_2 surrounding the rotor generally reduces the critical speed, it also leads to destabilizing forces on the rotor (e.g., Kim et al. [5]). The reduction in critical speed must be considered in the design of the TAC. In addition, to compensate for destabilizing forces that occur, the parameters of the AMB system must be adjusted. This must be taken into account especially for the start and stop procedure, since large changes in the fluid properties occur here due to the extended operating range. The procedure is described for the sCO2-HeRo cycle with the improved TAC and can be transferred to the NPP-scale heat removal system.

In addition, the repeatability of the pressure ratio measurements was demonstrated in comparison to the measurements performed in the sCO2-Hero project. Since the aerodynamic design was not changed for the new TAC, this is an expected result. The pressure ratio measurements match well with the original measurements from the sCO2-HeRo project, but have much higher accuracy. From this, it can be concluded for the first time that the CFD calculations, which are also used to validate a centerline calculation of compressor performance maps for the TAC for the NPP (Ren et al. [6]), predict the pressure ratio slightly too high. This must also be considered when evaluating the operating range of the NPP heat removal system.

Due to the foreseeable challenges in the design and operation of AMBs, a feasibility study on aerostatic gas bearings for sCO_2 is also being conducted. For this study, a calculation code is developed by TU Kaiserslautern (as subcontractor) and validated by measurements in a test rig. The aerostatic gas bearings have porous sleeves through which sCO_2 is forced to create a lubricating film. These bearings have several advantages over conventional oil-lubricated bearings, including longer operating time, more operating cycles due to lower friction, and no contamination of the working fluid. Unlike conventional dynamic bearings (e.g. foil bearings), no static friction has to be overcome during start-up and the transition from mixed friction to liquid friction is eliminated. Even at low speeds, a lubricating film is formed and the stick-slip effect does not occur. The

experiments will be carried out with a new test rig. This will be connected to the SCARLETT circuit at the partner USTUTT and supplied with sCO_2 by the latter. Finally, the validated code allows the accurate determination of the load carrying capacity of these bearings and can support the design of the TAC in Task 4.2 by providing another bearing option for sCO_2.

4 Improvement of the sCO2-HeRo turbomachine

4.1 Summary of reasons and expected effects of the turbomachine improvement

Experiments in the sCO2-HeRo project clearly identified grease-lubricated ball bearings in the original TAC as a problem. In particular, the fact that the sCO_2 can extract the oil from the grease prevents these bearings from operating under supercritical conditions. In fact, any bearing operating in sCO_2 must dispense with conventional oil-based lubricants. To overcome this challenge, there are two options. The first option, which was used in the sCO2-HeRo project and is a standard approach for other applications, is to operate the bearings at subcritical conditions, particularly at subcritical pressure. The second option is to switch to alternative bearings that do not require oil-based lubricants and either use sCO_2 itself as a lubricant (e.g. gas bearings) or do not require a lubricant (e.g. magnetic bearings). The advantage of the second option is obvious. While operating the bearings at subcritical pressure requires the implementation of a low-pressure operating limit below the critical pressure of 74 bar and the operating pressure, the second option does not require such a pressure limit. That is, no additional compressor or pump is required to lower the pressure in the machine housing and return the inevitable leakage to the circuit. Similarly, there is no need for the safety relief valve to ensure subcritical pressure. This increases the simplicity and robustness of the system, since failure of the additional compressor results in loss of CO_2 inventory through the additional safety relief valve. In this case, the system is no longer operational and must be refilled. Furthermore, the parallel operation of two compressors is an additional control challenge and is omitted in this case. Last but not least, the lower pressure differential across the labyrinth seals on the impeller disc reduces internal leakage losses in the improved TAC. Therefore, simple labyrinth seals (compared to dry gas seals with a very low leakage rate) can be used, resulting in a more robust TAC.

4.2 Overview on new turbomachine design

Figure 1 shows two 3D-printed 1:1 scale models of the original TAC (Hacks et al. [1]) as well as the improved design on the right. Pictures of the latter are presented in Figure 13 in Appendix B showing the improved TAC during commissioning tests with air (left) and integrated in the sCO2-heRo cycle (right). Both, the original and improved TAC follow the same concept of an integral design. This design features, from left to right, a compressor (blue), generator (yellow), and turbine (red) on a single shaft (light gray) in a hermetic housing (dark gray). The compressor and turbine stator and their seals are colored green. In the improved TAC developed in Task 4.1 of the sCO2-4 NPP project, AMBs replace the ball bearings. The AMBs in the TAC on the right, supplied by subcontractor MECOS AG, consist of the thrust bearing (orange) with the thrust disk (black) and the two radial bearings (beige) in combination with position sensors (white) with their rotor sleeves (black) and safety bearings (metallic) (see also Barreault [7]). Figure 1 gives only limited information about the change in machine size. The magnetic bearings are wider due to their limited load capacity, the additional position sensors and the safety bearings. The latter are ball bearings with solid lubrication[1] and already have the same width as the bearings in the original design. Therefore, as shown in Table 1, the overall length of the rotor and especially the length of the protrusion between radial bearings and impellers is longer. In order to keep the design rotor dynamically comparable, i.e. not having a critical speed below the design speed, the shaft

[1] Solid lubricants can be used in sCO_2 and are suitable for safety bearings, which are only used for a few seconds if the magnetic bearing fails. However, they are not suitable for supporting a high-speed rotor for a longer period of time

diameter is increased accordingly and the thickness of the impeller is reduced for a reduction in impeller weight. Therefore, the rotor can still be considered subcritical in terms of rotor dynamics, even though the length of the rotor and the entire TAC increases by about 20 % while the casing diameter remains constant. Another feature that was not present in the original TAC is the thrust disk. Its diameter was minimized to reduce frictional losses with the surrounding sCO_2 and axial thrust caused by the pressure distribution across the disk. Nevertheless, it is about 50 % larger than the compressor impeller and its contribution to ventilation losses and axial thrust must be considered. The new design also brings new tubes and measurements and control valves, shown in red in the P&ID in Figure 12 in Appendix A. The additional pipes with valves TK02 S201 - TK02 S205 are introduced to compensate for the axial thrust due to the flow direction at the thrust disk (centrifugal vs. centripetal). They also allow variation of the density of sCO_2 within the TAC and ensure sufficient cooling, especially of the turbine-side bearing and the generator. Furthermore, the updated P&ID shows the additional measurements to monitor the thermodynamic properties of the CO_2 inside the TAC. Not shown, however, are measurements of the AMB system, which measures the position of the rotor and the electrical parameters of the bearings to evaluate the forces acting in the bearings and thus the interaction of sCO_2 with the rotor.

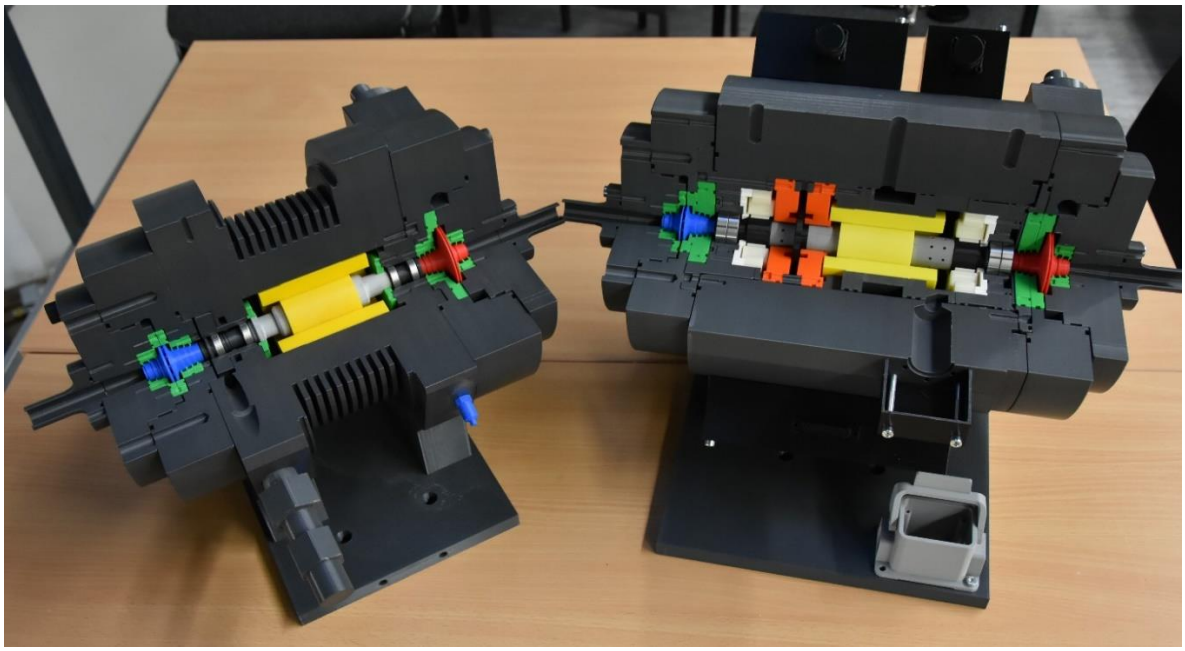

Figure 1: 3D-printed 1:1 scale models of TACs developed in the sCO2-HeRo project (left) and their improved version from the sCO2-4-NPP project (right) for laboratory-scale experiments [8]

Table 1: Change of rotor dimensions for application of magnetic bearings

Dimension	Change in Size / %
Total rotor length	120
Radial bearing distance	89
Overhang of compressor impeller	118
Overhang of turbine impeller	138
Shaft diameter at radial bearings	167
Mean thickness of compressor hub disk	49
Mean thickness of compressor shroud disk	44
Mean thickness of turbine hub disk	47
Mean thickness of turbine shroud disk	47

5 Operation of improved turbomachine

5.1 Operation of magnetic bearings

AMBs have not yet been tested in detail in sCO_2. Publications (e.g. by Kim et al. [5]) suggest that destabilizing forces on the rotor due to sCO_2 could be problematic for successful operation and therefore need to be considered in rotor dynamic design calculations. In particular, the sCO_2 in the long, narrow, cylindrical gap between the generator rotor and stator (yellow parts in Figure 1) interacts with the rotor and causes forces that contribute to destabilization of the system. These forces can be expressed by negative stiffness coefficients and calculated using a rotor dynamic model of the gap. The overall rotor dynamic model takes into account these coefficients and, in addition, consists of the rotor itself and the control unit of the AMBs. It is validated in the experiments by measuring the deflection of the rotor due to an excitation by the AMB system. These measurements confirm that the model generally represents the system well. Therefore, the system model can be used to optimize and adjust the AMB controller. In the experiments, the maximum speed of about 40,000 rpm was achieved in CO_2 with a density of about 200 kg/m³. In contrast, about 30,000 rpm were achieved with a density of about 650 kg/m³ at the compressor inlet. In contrast to conventional turbomachines operated with air, the AMB controller was modified for this purpose so that it switches internal control parameters at certain speed limits in order, for example, to increase the bearing stiffness and thus compensate for the negative stiffness caused by the sCO_2 in the cavities. It should be noted that the fluid forces or negative stiffness acting on the rotor increase with the density of the sCO_2. From this it can be seen that the controller must also be adapted to the conditions of the CO_2 in the cavities. This is an important requirement for the design and operation of the TAC even for the NPP scale.

In addition, the critical speed decreases as the density of sCO_2 in the rotor-stator cavities increases. This must also be considered in the design of the TAC. In this case, the TAC operates sub critically, i.e. the design speed of 833 Hz is below the first critical speed of about 1.050 Hz. Thus, it is only necessary to guarantee that the critical speed does not drop to the design speed. However, if a TAC were to be operated at a design speed above the first critical speed, this would be critical. In this case, the AMB system control would need to be adjusted at the critical speed and prolonged operation in this speed range should be avoided. However, since the sCO_2 conditions affect the critical speed, it would be necessary to repeatedly recalculate the actual critical speed based on the sCO_2 conditions during operation. Therefore, a subcritical design in terms of rotor dynamics is considered advantageous and recommended for NPP-scale TAC.

However, beyond this, overall control of the density within the TAC cavities is beneficial and also possible by controlling the cooling and leakage flows within the improved TAC. In this design, a cooling flow is introduced via valves TK02 S201 and TK02 S202. Care is taken to supply a cooling current as low as possible and at the same time to keep within the temperature limits of the bearings and the generator, in this case about 150 °C. The cooling current is then discharged via the valve TK02 S205 visible in Figure 12. Bearings and generator are heated by internal electrical losses and the hot leakage flow from the turbine, which mixes with the cooling flow introduced via the TK02 S201 valve. Low density within the TAC, controlled with the aid of the cooling mass flow, can also reduce destabilizing forces, especially from the sCO_2 in the generator gap, and at the same time reduce the friction losses of the rotor with the sCO_2. In addition, it results in less sensitivity of the pressure distribution at the thrust disk to the rotation of the rotor and thus easier control of the axial thrust. Therefore, there are two requirements for the density inside the TAC. It must be measured and generally be as small as possible to reduce frictional losses, negative stiffness and axial thrust. However, a lower cooling effect of the CO_2 must be accepted, which may require motors and bearings with a higher temperature limit.

5.2 Improved measurements

The additional mass flow and density measurement installed at the compressor discharge allows improved monitoring of the leakage and cooling flow rates as well as the compressor pressure ratio. Since the geometry of the seal is the same, the same dimensionless leakage coefficient ζ can be used. It is determined according to the formulation of Lüdtke [9] (p. 217) and describes flow through a seal independent of thermodynamic properties and pressure ratio. In fact, a value of about 0.7 was obtained for both the original and the improved TAC. This means, as shown by the red line in Figure 2, that the leakage flow rate is more than 50% smaller at speeds below 20,000 rpm. This is caused by the fact that the pressure ratio across the seal is closer to one for the improved TAC with magnetic bearings (black line in Figure 2), because this TAC does not require subcritical pressure downstream of the seal in the area of the bearings. Since the difference in pressure ratios represented by the difference in the gray and black lines in Figure 2 is greater at low speed, the reduction in leakage flow rate is also greater here.

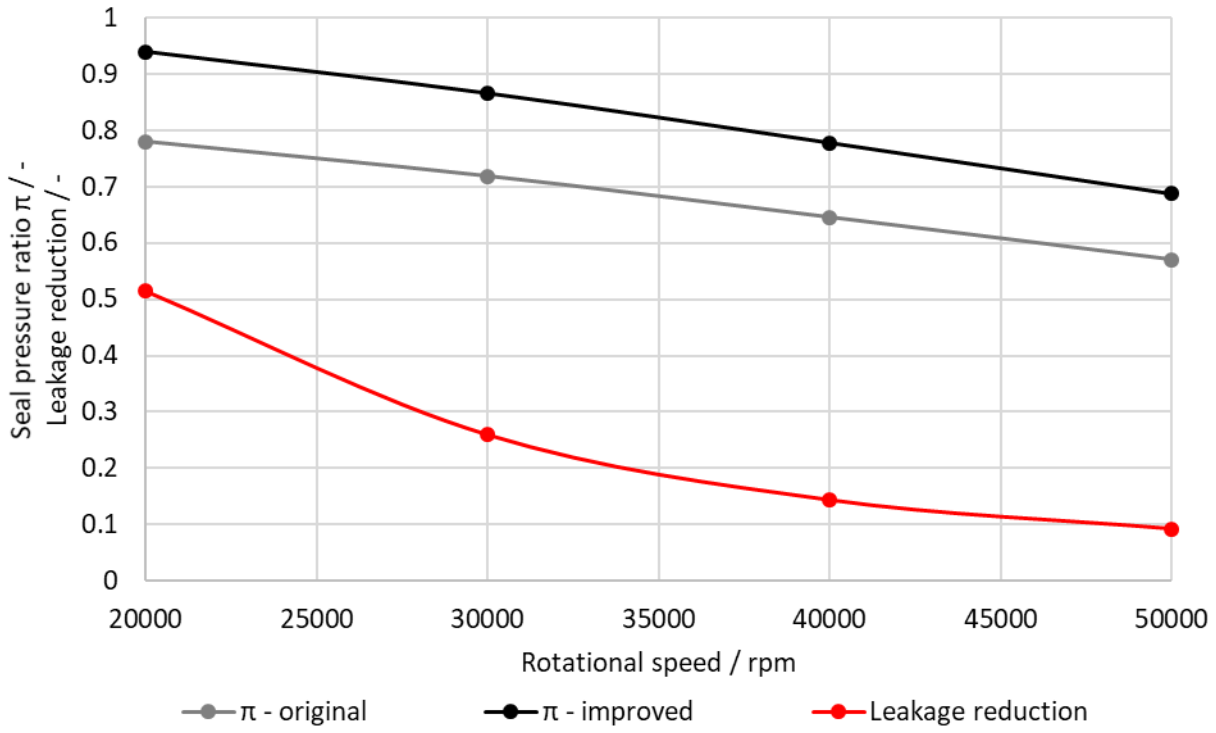

Figure 2: Leakage reduction due to lower pressure ratio by dispensing with additional compressor

Figure 3 compares the pressure ratio plotted versus mass flow at the impeller inlet of the compressor with measurements from the original TAC and CFD predictions. The comparison is made at the thermodynamic design point and all measurements are scaled using similarity laws as described by Hacks et al [8]. The pressure ratios are comparable to those measured in both the SUSEN cycle [8] and the sCO2-HeRo cycle [10] with the original machine, demonstrating the reproducibility of the measurement results. Furthermore, the uncertainty of the measured pressure ratio is now below 0.001 and not in the range of 0.02 to 0.03 as before. While in the previous measurements the CFD results were within the error bars, the lower uncertainty of the new measurements now suggests that the CFD calculations slightly overestimate the pressure ratio. Since the pressure ratio defines the operating point of the cycle, a margin for the pressure ratio must be considered in NPP-scale cycle calculations. Based on this, CFD calculations and centerline models (Ren et al. [6]) are still considered valid for creating maps for the NPP-scale TAC.

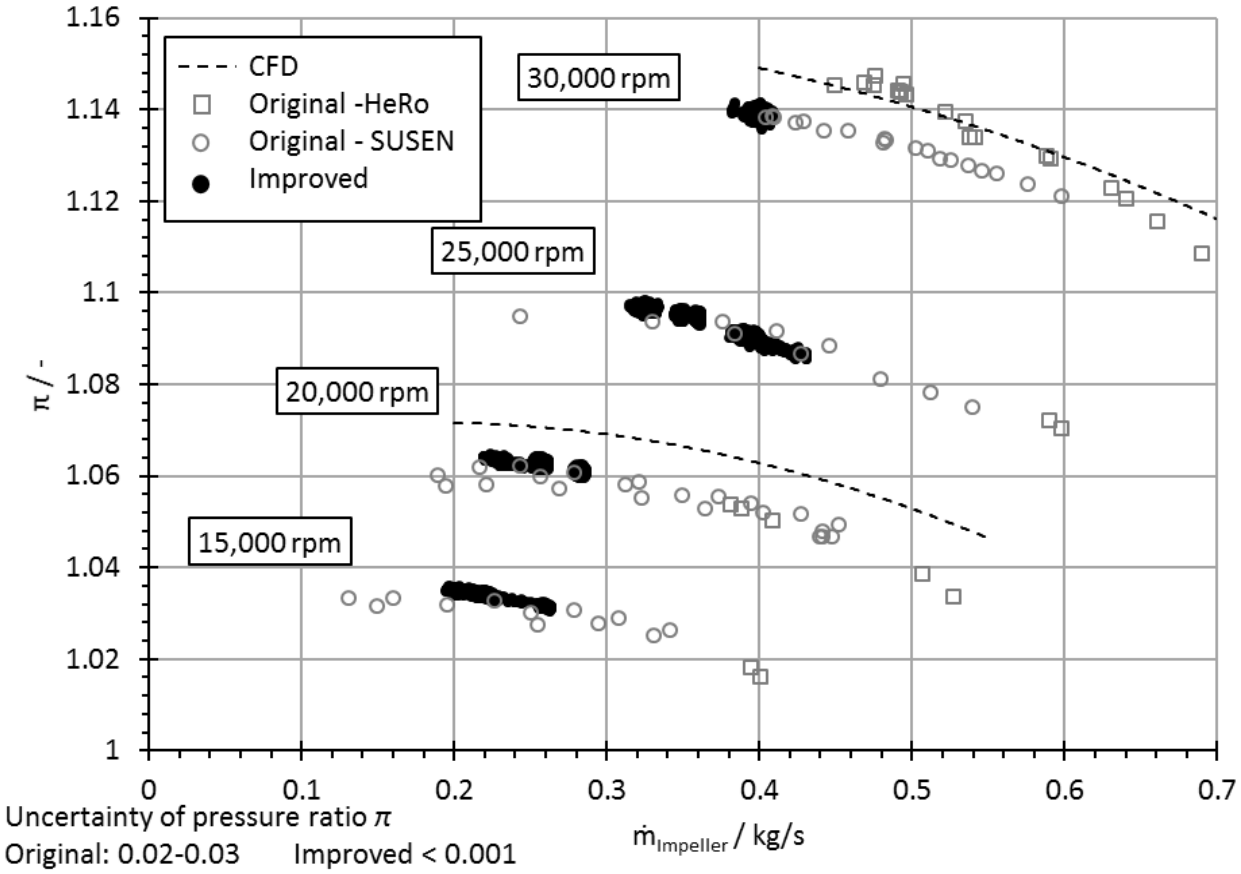

Figure 3: Comparison of the pressure ratio versus mass flow at the impeller inlet of the improved TAC's compressor with previous measurements from the sCO2-HeRo project and CFD predictions

5.3 Improved cycle design

The sCO2-HeRo cycle is operated with the improved TAC without the additional piston pump (PP) under normal conditions and the safety relief valve, which was previously installed to ensure subcritical pressure at the ball bearings, was removed. With the safety relief valve limiting the pressure in the original TAC to a maximum of 67 bar, there was a risk of inventory loss due to PP malfunction. Further, the compressor inlet pressure was limited by the limited capacity of the PP. While the original TAC did not allow compressor inlet pressures above 78 bar, the improved TAC allows compressor inlet pressures up to 90 bar (see Figure 4). Therefore, the operating range is wider and the control of the entire circuit is simpler and more robust. This is one of the main requirements for the NPP-scale heat removal system and thus another advantage of using AMBs.

5.4 Start and Stop procedures

One issue that needs to be discussed for the successful operation of the heat removal system with sCO_2 is the startup and shutdown of the system. Therefore, the constraints on start and stop procedures due to the application of AMBs will be investigated. The following chapter shows the start and stop strategy for the sCO2-HeRo cycle with the improved TAC, which can be applied to the NPP scale considering the limitations of the operation of AMB in sCO_2. Figure 4 sketches the processes of startup with a thick dark red line, improved TAC

normal operation with a thick black line, and shutdown with a thick blue line in a T-s diagram as an example for operation on February 25, 2021, showing conditions based on measurements downstream of the heat sink (UHS) closest to the two-phase region. Since the improved TAC is temporarily disconnected from the circuit during the startup and shutdown procedures, the inlet condition of the compact heat exchanger (CHX) is shown there, as marked in Figure 4. The diagram also includes, in light gray, the conditions at the compressor inlet during normal operation on various other test days. Thus, Figure 4 gives an impression of the thermodynamic conditions to be considered during the various operating phases of the sCO2-HeRo cycle.

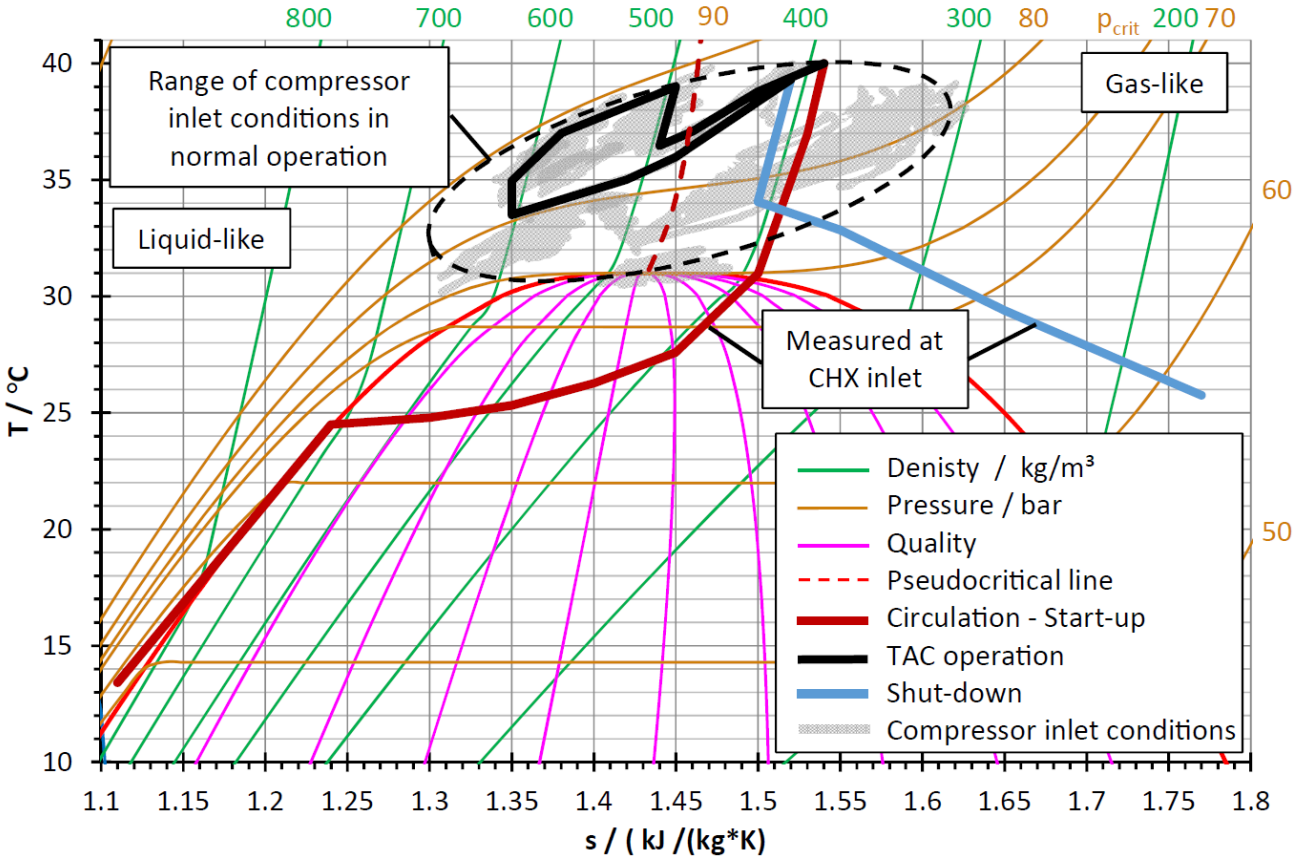

Figure 4: Operating conditions during start-up (heating up), TAC operation and shutdown (cooling down) - example from February 25, 2021

5.4.1 Start procedure

Start-up tests showed a problem in cold shutdown conditions when the CO_2 in the closed loop is in dual phase. The improved TAC is installed with the rotor in the horizontal direction and droplets of liquid CO_2 form and collect in the gaps between the rotor and stator. Therefore, the fluid properties around the rotor are very inhomogeneous when the cycle is not in operation. The influence of the inhomogeneous distribution of liquid and gaseous CO_2 is sufficient to prevent lift-up of the rotor even without rotation. At least during the limited period of commissioning, this could not be remedied. However, even if this problem could be solved by further optimization of the AMB controller, it seems more effective to avoid these conditions during operation. Therefore, for the tests in the sCO2-HeRo loop, conditions with two-phase CO_2 in the improved TAC were avoided, resulting in the following start-up strategy.

First, using the PP that was required for the original TAC to maintain subcritical pressure at the bearings, CO_2 is circulated through the loop to slowly heat it in the slave electrical heater (SEH) and bring the loop to supercritical pressure and temperature above 74 bar and 31 °C (thick red line in Figure 4). During this process,

the internal leakage recirculation of the TAC is connected to the inlet of the PP via valves TK02 S101 and TK02 S205 (see Figure 12). This results in a leakage flow across the seal of the turbine, which is used to heat the improved TAC. The thick red line in Figure 4 begins when the flow meter at the CHX first measures a mass flow of liquid CO_2 forced out of the UHS by the circulation of CO_2 with the PP. When the liquid and gaseous CO_2 are evenly distributed in the circuit, the mass of CO_2 in the circuit can be estimated and further pressure increase is possible only by adding heat in the CHX or SEH. Circulation and heating will continue until the compressor inlet conditions are well above the critical pressure and temperature. At the point where the thick black line begins, the compressor takes over the task of circulating the sCO_2. To do this, the rotor is lifted and rotated at a low speed of less than 10,000 rpm. At the same time, the PP is stopped and all the valves used to separate the TAC from the circuit are fully opened, while at the same time the compressor bypass is closed. Once all valves are set to operate with the TAC instead of the PP, the speed is increased until the CO_2 circulates through the open turbine bypass valve. Note that during the time when the PP is not operating and the compressor is still rotating at low speed with the bypass open, a natural convection cycle occurs as the UHS is below the SEH and collects the sCO_2 by cooling it and increasing its density. This means that the flow direction between the SEH and the UHS is reversed via the compressor bypass valve. Only after increasing the speed of the TAC and closing the compressor bypass valve, the intended flow direction is re-established. It should be noted that the switching process is limited in time by the cooling of the sCO_2. Should it take too long, the circuit pressure will again drop below the critical pressure of 74 bar, resulting in phase separation. The latter, in turn, can lead to an instability of the controller and thus to a sinking of the rotor into the safety bearings. However, once the compressor is circulating the sCO_2, the speed can be increased and the turbine bypass closed, taking into account the compressor surge limit. The cycle and the improved TAC are now in normal operation. The compressor is operating under the conditions enclosed by the black dashed lines. Since the mass of CO_2 in the circuit is constant in the example, the higher density compressor operating conditions marked by the black line refer to operation at higher SEH discharge temperature. Operating the compressor at inlet conditions different from the example shown requires a different mass of CO_2 in the loop. The light gray dots in Figure 4, framed by the dashed lines, correspondingly show the compressor inlet conditions of some other test runs. Since the achievable operating conditions depend directly on the mass of CO_2 in the circuit, it is generally of great importance to monitor it at all times. By changing the compressor inlet condition, it determines the compressor pressure ratio and thus the range of self-sufficient operation of the system (higher density → wider range). However, in the sCO2-HeRo cycle, especially in the cold standstill condition when the CO_2 is two-phase, it is not possible to quantify the mass of CO_2 because the level of liquid CO_2 in the different components, especially in the UHS and the SEH, cannot be determined. Therefore, the average density in the sCO2-HeRo loop cannot be determined until the CO_2 is in a supercritical single-phase state after startup or until liquid and gaseous CO_2 are at least evenly mixed. If CO_2 is lost during shutdown due to a leak in the loop (small leaks are almost unavoidable), setting the desired operating point may not be possible. Therefore, it must be ensured for the system at NPP-scale that the CO_2 mass in the cycle can be determined at any time.

In summary, during startup, it must be ensured that the CO_2 is homogeneous throughout the TAC and that there are no sudden density changes in the rotor-stator cavities due to the separation of liquid and gaseous CO_2. Thus, to operate the system in a NPP, a warm-up procedure must also be established or the system must be kept in a heated "standby" state continuously, e.g. using waste heat. The latter also simplifies the monitoring of the CO_2 mass in the circuit, since the CO_2 is then present in a single phase.

5.4.2 Stop procedure

The main requirement to bring the system back to cold standstill is to cool all components down to a safe level and avoid any two-phase CO_2 in the improved TAC while it is still spinning. In the sCO2-HeRo circuit, the electric heater has a solid aluminum core that stores a large amount of energy that must be transported outside by circulating CO_2 through the circuit to the cooler. Therefore, the TAC continues to run when the heater is turned off. By opening the turbine bypass, the CO_2 flow is kept sufficiently high while the speed can be reduced. The cooling capacity of the air cooler must be adjusted so that the accumulated mass in the cooler does not become so large that the pressure falls below the critical pressure of 74 bar. Only when the compressor inlet conditions transits from liquid to gaseous sCO_2, i.e. the pseudocritical line in Figure 4 is crossed, can the cooling power be increased. This is marked by the transition from the thick black line to the blue line. Increasing the UHS fan speed in combination with reducing the TAC speed at this point can cause a drastic change in thermodynamic conditions, which can be seen by the thick blue line in Figure 4. Circulation of CO_2 continues at a low flow rate with the UHS fan speed maintained at a high level until the SEH outlet temperature reaches a safe level and the TAC is stopped.

6 Mitigation – Aerostatic gas bearings

6.1 Overview of aerostatic gas bearings

Hydrostatic gas bearings using sCO_2 as lubricant are investigated as mitigation to AMBs to ensure that a validated bearing concept is available for the NPP-scale TAC to be designed in Task 4.2 of the project. The subcontractor TU Kaiserslautern has developed several models for the design of aerostatic porous bearings described by Böhle et al [11] and Schimpf et al [12]. Based on these models, an improved model called Full Darcy Plus (Figure 5) was developed that incorporates the properties of the fluid. In each iteration step, the density and viscosity of the fluid are obtained from the CoolProp substance database. The model also takes into account the geometry of the pressure chambers, improves the physical modeling of the lubricant film and the calculation of bearing performance.

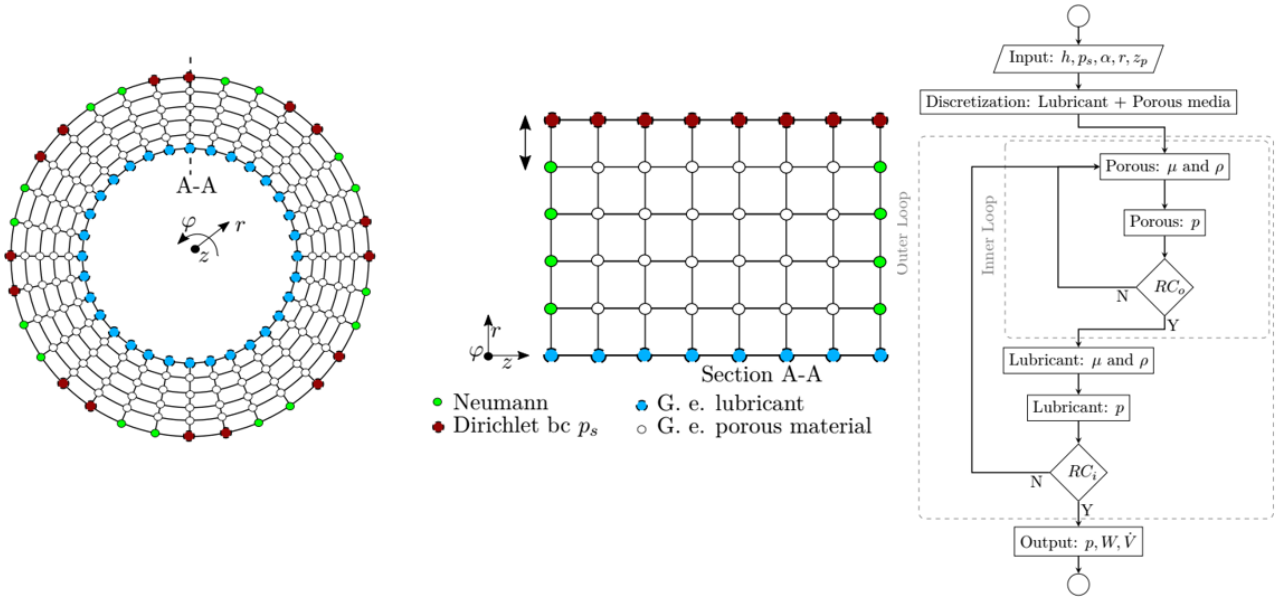

Figure 5: Full Darcy Plus model

For experimental validation of the results, the bearing test rig of the Technical University of Kaiserslautern is coupled with the sCO_2 test rig (SCARLETT) of the University of Stuttgart. The operation of the test rig is shown schematically in Figure 6, while a schematic view and images of porous bearing sleeves are shown in Figure 7. In the schematic view in Figure 6, a stepper motor gradually applies a radial force to the test bearing housing. The radial force, which transmits the eccentricity of the bearing, is determined by an s-shaped force sensor. The displacement sensors are positioned both vertically and horizontally to determine the gap width as well as the offset. An electric motor drives the test shaft. A flexible elastomer coupling compensates for minor misalignment between the motor and shaft. The predominantly vertical eccentricity of the shaft in relation to the support bearings is measured with two additional displacement sensors. These provide information on whether contact between the support bearings and the shaft is imminent. The compressed air from the support bearings and the test bearing is treated by a two-stage particle filter system and a dryer. The filtering of the lubricating medium is to prevent clogging of the porous material and to allow repeated measurement. The flow rate is measured with a Coriolis flowmeter, which has an error of 0.035 %. The accuracy of the pressure transmitters is 0.03 % full scale output (FSO). The maximum linearity error of the displacement

sensors is 1.2 µm. The bearing test rig was first put into operation with air, the construction and some pictures can be seen in Figure 8.

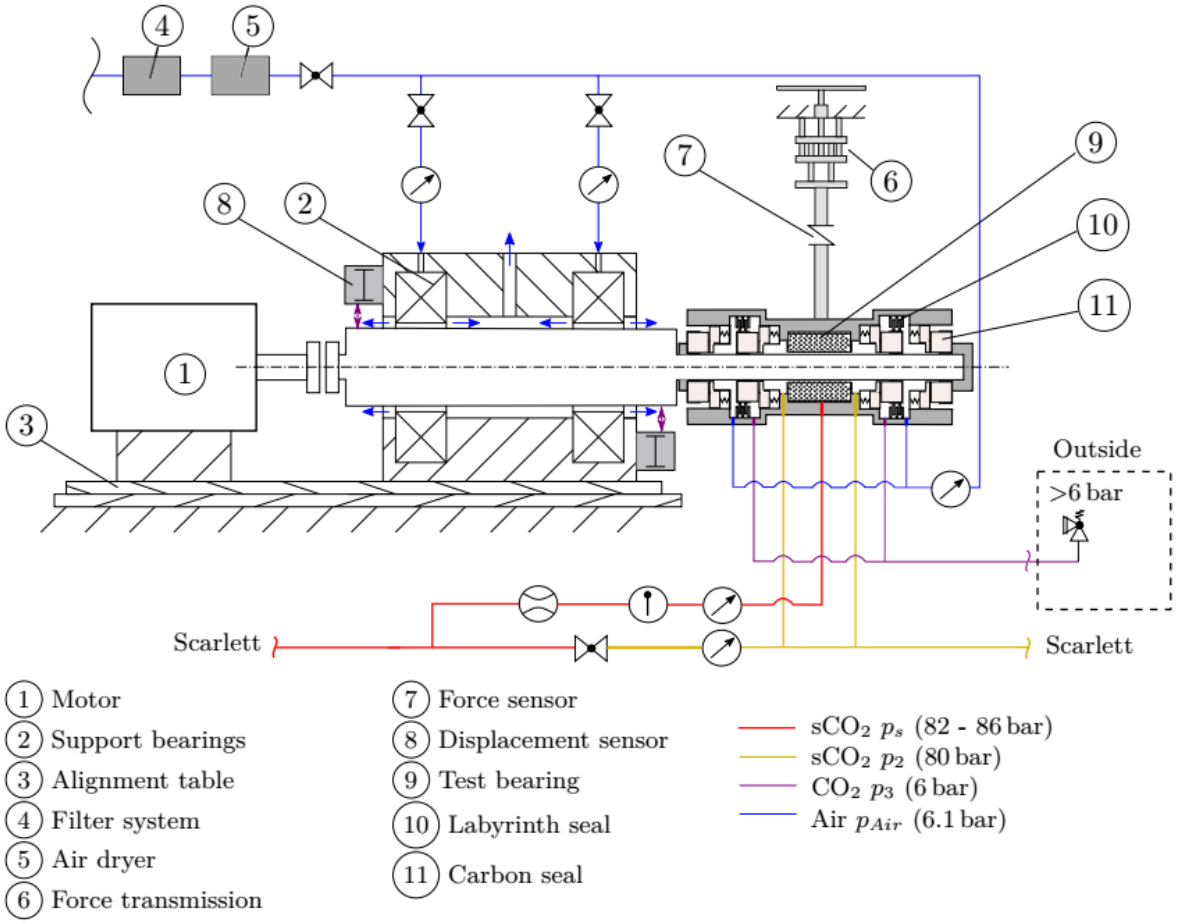

Figure 6: Concept of the aerostatic gas bearing test rig

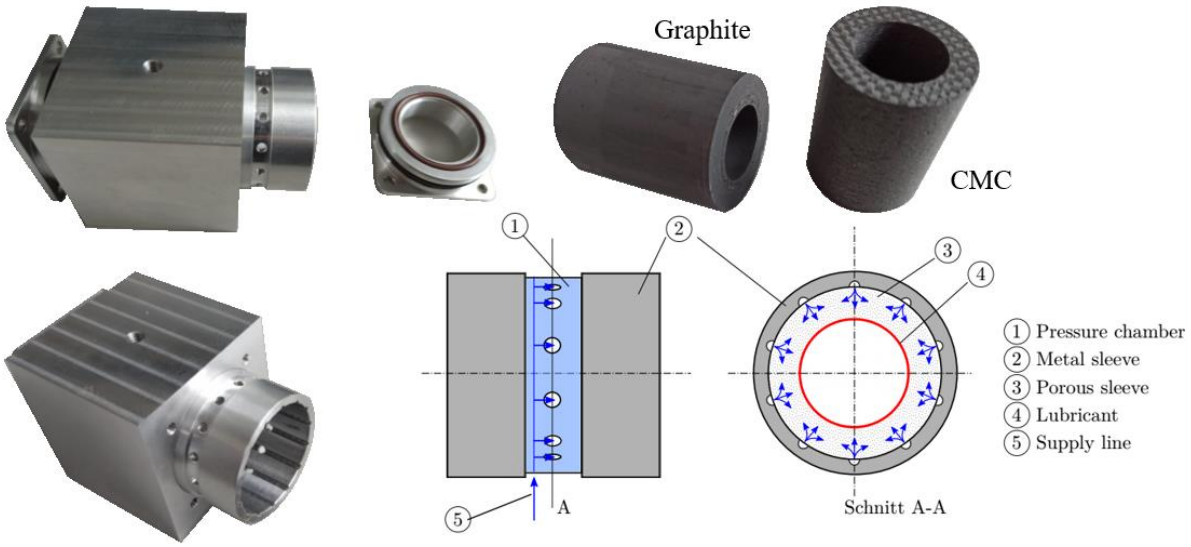

Figure 7: Aerostatic bearings with porous sleeves

Figure 8: Aerostatic gas bearing - bearing housing (top left), seals (top right) and test rig during initial air commissioning tests (bottom)

6.2 Results aerostatic gas bearings

Figure 9 shows the calculated load capacities *W* compared to the dimensionless eccentricities ϵ for CO_2 with the three models developed by the subcontractor TU Kaiserslautern. Increasing the complexity of the models leads to lower values in the corresponding static performance parameters, caused by the change in pressure distribution in the porous medium shown in Figure 10. Modeling the pressure chamber leads to a more non-uniform distribution of the fluid in the porous body in the Full-Darcy-Plus model. An increase in the pressure difference leads to an increase in the bearing capacity and flow rate, which is also shown by the measurements of Mokhtar et al [13] to validate the Full-Darcy model in Figure 11. As part of the preliminary tests, measurements were made with air lubrication, which are also shown in Figure 9. The radial force on the test bearings was increased until the friction between the shaft and bearing increased. It indicates the transition from liquid friction to mixed friction, which indicates the limit of load capacity. The supply pressure was set at 4 and 6 bar. Since no seals were used initially, atmospheric pressure prevailed at the outlet. In the further

course, the radial load is reduced and the eccentricity is determined with laser triangulation sensor. The first series of tests showed the bearings to be functional and no instabilities (jackhammer). Furthermore, the load carrying capacities of the bearings for air are in the expected range.

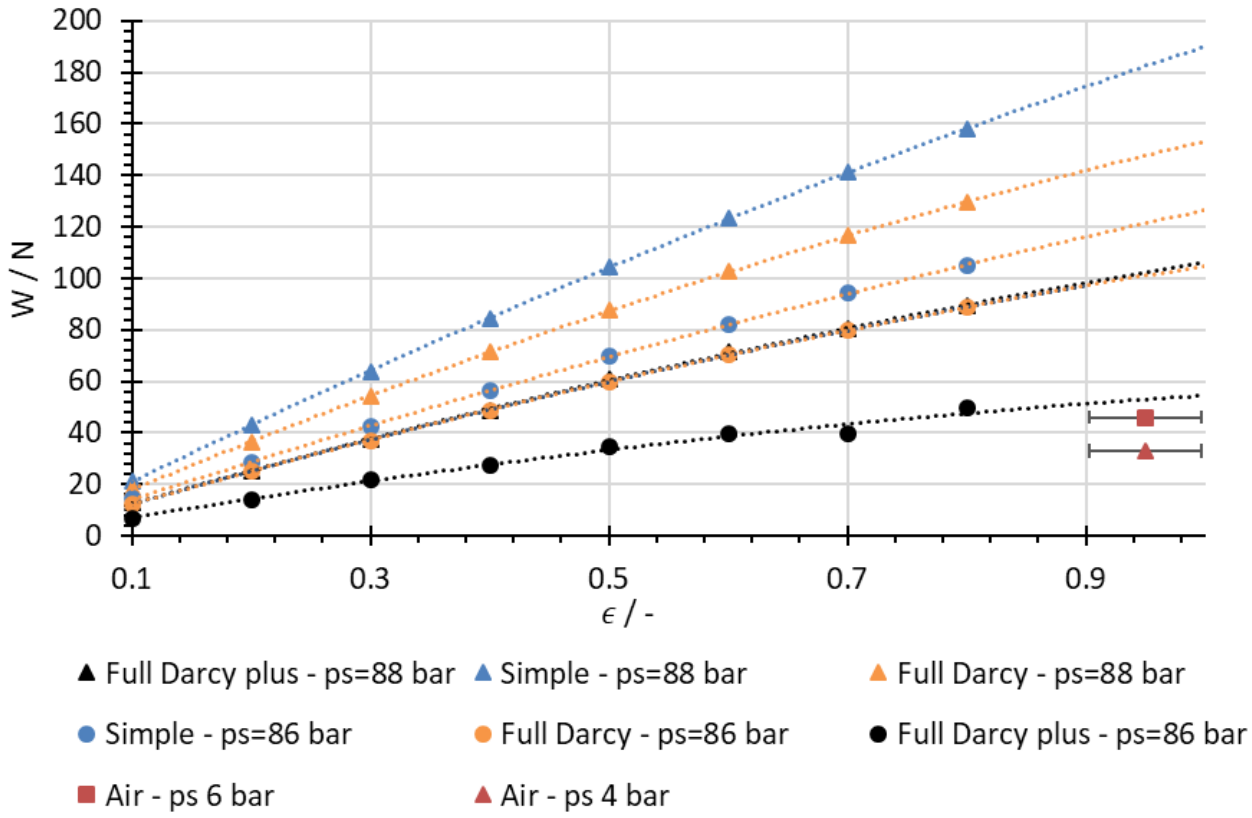

Figure 9: Prediction of the load caring capacity at 8000 rpm

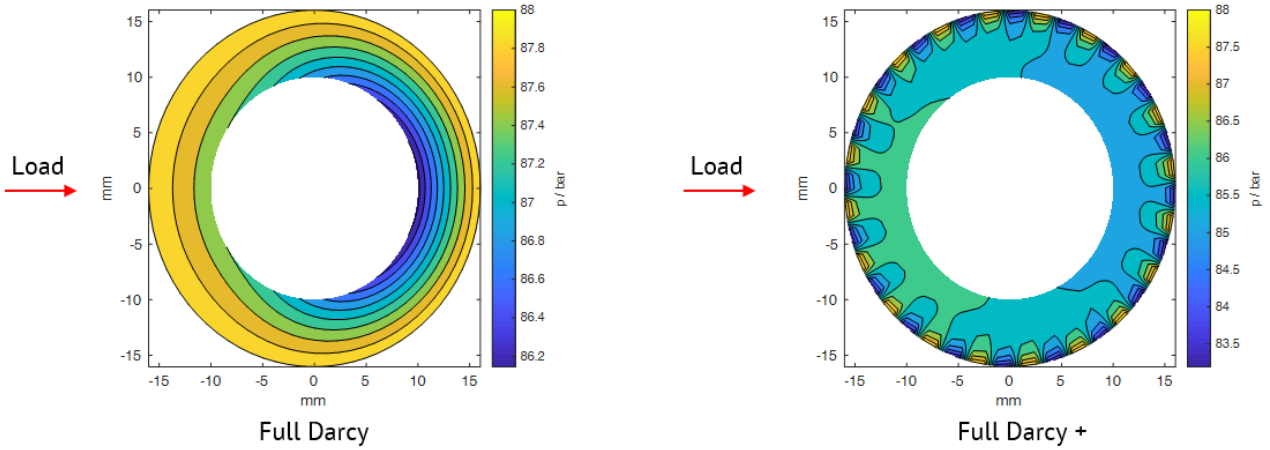

Figure 10: Pressure distribution in a porous sleeve

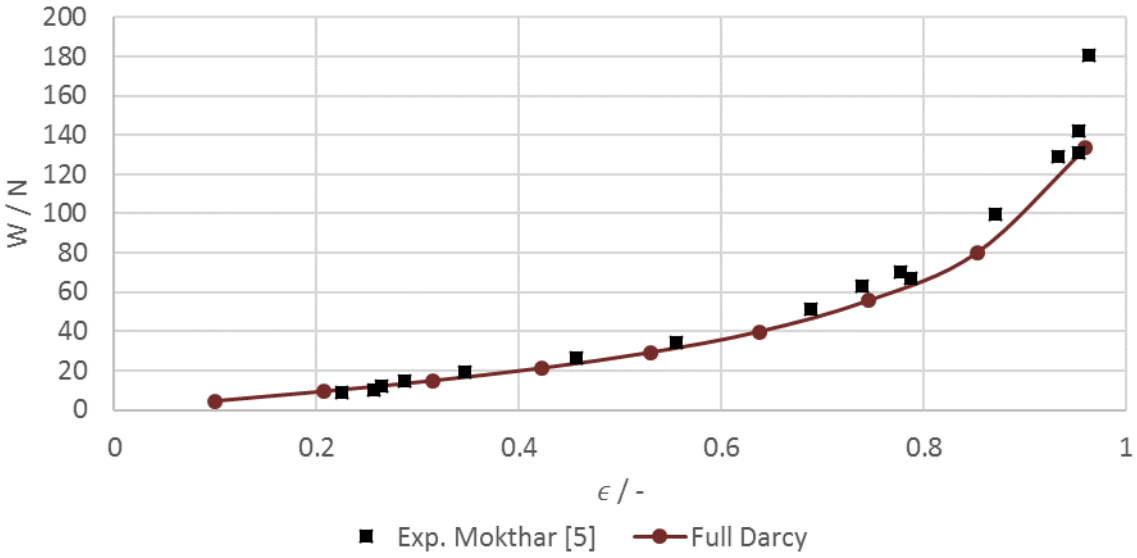

Figure 11: Validation numerical results with measurements by Mokhtar et al. [13]

7 Conclusion

The deliverable presents the TAC design changes and experimental results of an improved TAC with AMBs for operation in the sCO2-HeRo cycle. Based on these results, recommendations for the design and operation of the TAC in the NPP-scale heat removal system are formulated, and a suitable starting and stopping procedure is described.

The experiments with the improved TAC lead to the conclusion that the operation of the AMB with a rotor fully immersed in sCO_2 is challenging, since the control parameters of the AMB must take into account the sCO_2 characteristics to ensure stable operation. However, consideration of these during commissioning proves that AMBs are a suitable technology for TACs with sCO_2 throughout the machine casing and thus for the heat removal system. Additionally, aerostatic gas bearings, which are being investigated as mitigation to AMBs, also promise to be a suitable technology for operation in sCO_2. This eliminates the need for additional pumps and a subcritical low pressure boundary below the design operating pressure, paving the way for a more robust and simpler design of the heat removal system in general. A suitable start/stop strategy to avoid two-phase CO_2 in the rotor-stator cavities has been developed and can be transferred to the NPP-scale heat removal system. In addition, the mechanical and aerodynamic design tools are revalidated by showing the reproducibility of previous measurements and a good agreement between model prediction and measurements, which increases the confidence in the design of the NPP-scale TAC.

Therefore, this deliverable provides the information for an appropriate TAC design for Task 4.2 as well as recommendations for the operation of the NPP-scale heat removal system for work package 5, thus fully meeting the objective of Task 4.1 and this deliverable.

8 References

[1] Hacks A., Schuster S., Dohmen H. J., Benra F.-K., and Brillert D., 2018,“Turbomachine Design for Supercritical Carbon Dioxide Within the sCO2-HeRo.eu Project,” Journal of Engineering for Gas Turbines and Power, **140**(12).

[2] Brun K., Friedmann P., and Dennis R., Eds., 2017. *Fundamentals and applications of supercritical carbon dioxide (sCO2) based power cycles*, Woodhead Publishing, Oxford.

[3] Miol M. de, Bianchi G., Henry G., Holaind N., Tassou S., and Leroux A.,“Design of a single-shaft compressor, generator, turbine for small-scale supercritical CO2 systems for waste heat to power conversion applications,” *2nd European sCO2 Conference 2018*, DuEPublico: Duisburg-Essen Publications online, University of Duisburg-Essen, Germany, pp. 42–49.

[4] Wright S. A., Radel R. F., Vernon M. E., Rochau G. E., and Pickard P. S., 2010,“Operation and Analysis of a Supercritical CO2 Brayton Cycle,” Sandia report, SAND2010-0171, Albuquerque, New Mexico.

[5] Kim D., Baik S., and Lee J. I., 2019,“Investigation of Magnetic Journal Bearing Instability Issues in Supercritical CO2 Turbomachinery,” *Volume 3B: Fluid Applications and Systems*, American Society of Mechanical Engineers.

[6] Ren H., Hacks A. J., Schuster S., and Brillert D.,“Mean-line analysis for supercritical CO2 centrifugal compressors by using enthalpy loss coefficients,” *4th European sCO2 Conference for Energy Systems: March 23-24, 2021, Online Conference*, DuEPublico: Duisburg-Essen Publications online, University of Duisburg-Essen, Germany, pp. 68–77.

[7] Barreault S., 2021,“3D-printed 1-to-1 scale model of turbomachine,” https://www.sco2-4-npp.eu/3d-printed-1-to-1-scale-model-of-turbomachine/.

[8] Hacks A., Vojacek A., Dohmen H. J., and Brillert D.,“Experimental investigation of the sCO2-HeRo compressor,” *2nd European sCO2 Conference 2018*, DuEPublico: Duisburg-Essen Publications online, University of Duisburg-Essen, Germany, pp. 50–59.

[9] Lüdtke K. H., 2004. *Process centrifugal compressors: Basics, function, operation, design, application*, Springer, Berlin.

[10] Hacks A. J., Freutel T., Strätz M., Vojacek A., Hecker F., Starflinger J., and Brillert D.,“Operational experiences and design of the sCO2-HeRo loop,” *3rd European Conference on Supercritical CO2 (sCO2) Power Systems 2019: 19th-20th September 2019*, DuEPublico: Duisburg-Essen Publications online, University of Duisburg-Essen, Germany, pp. 125–137.

[11] Böhle M., Gu Y., and Schimpf A., 2019,“Two Flow Models for Designing Hydrostatic Bearings With Porous Material,” *Volume 3B: Fluid Applications and Systems*, American Society of Mechanical Engineers.

[12] Schimpf A., Gu Y., and Böhle M., 2020,“Analysis of Flow Models for Aerostatic Thrust Bearings with Porous Material,” JMEA, **10**(6).

[13] Mokhtar M.O.A., Rafaat M., and Shawki G.S.A., 1984,“Experimental Investigations into the Performance of Porous Journal Bearings,” *SAE Technical Paper Series*, SAE International400 Commonwealth Drive, Warrendale, PA, United States.

Appendix A Piping and Instrumentation Diagram

Figure 12 shows the updated P&ID of the sCO2-HeRo cycle used to accommodate the improved TAC with AMBs. Compared to the P&ID presented by Hacks et al. [10], the measurements marked by red frames were added. The additional valves (valves TK02 S201 - TK02 S205) are used to control the pressure distribution, density and temperature of the sCO_2 inside the machine. The additional pressure and temperature measurements monitor the thermodynamic conditions at different positions in the TAC. In Figure 12, the new measurements and valves are highlighted in red. In addition (not shown in Figure 12), the AMB system allows evaluation of the forces acting on the shaft by measuring the rotor positions and the current in the magnetic bearings.

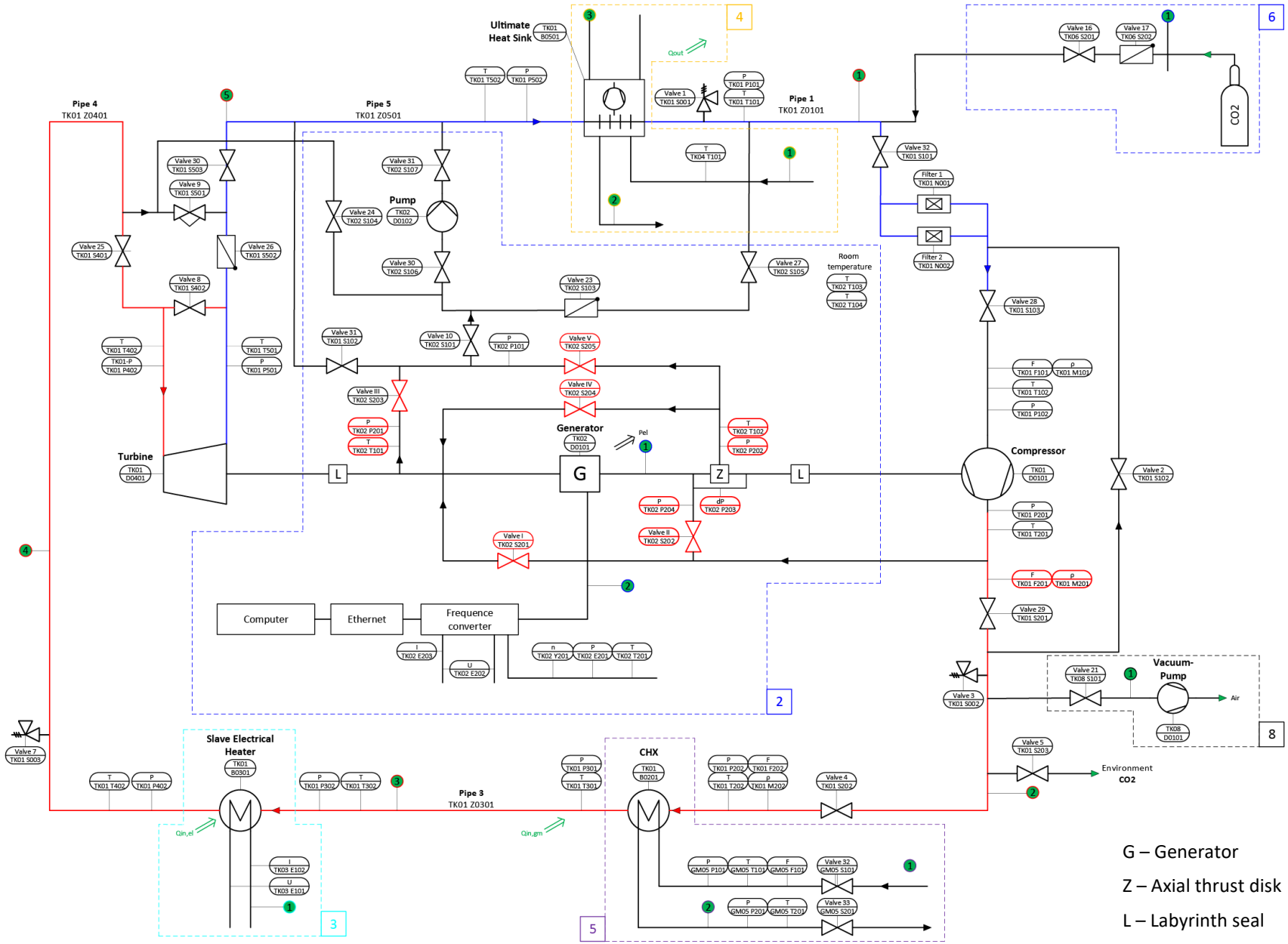

Figure 12: P&ID of the sCO2-HeRo cycle adopted for the improved turbomachine with magnetic bearings

Appendix B Pictures of improved turbomachine

Figure 13 presents the turbomachine during commissioning tests with air on the left and integrated in the sCO2-HeRo cycle on right. Both pictures show the same view. In the foreground are the new valves TK02 S201 – TK02 S205 and the new sensors according to Figure 12. The TAC itself is oriented in a way that the compressor is on the right and the turbine on the left.

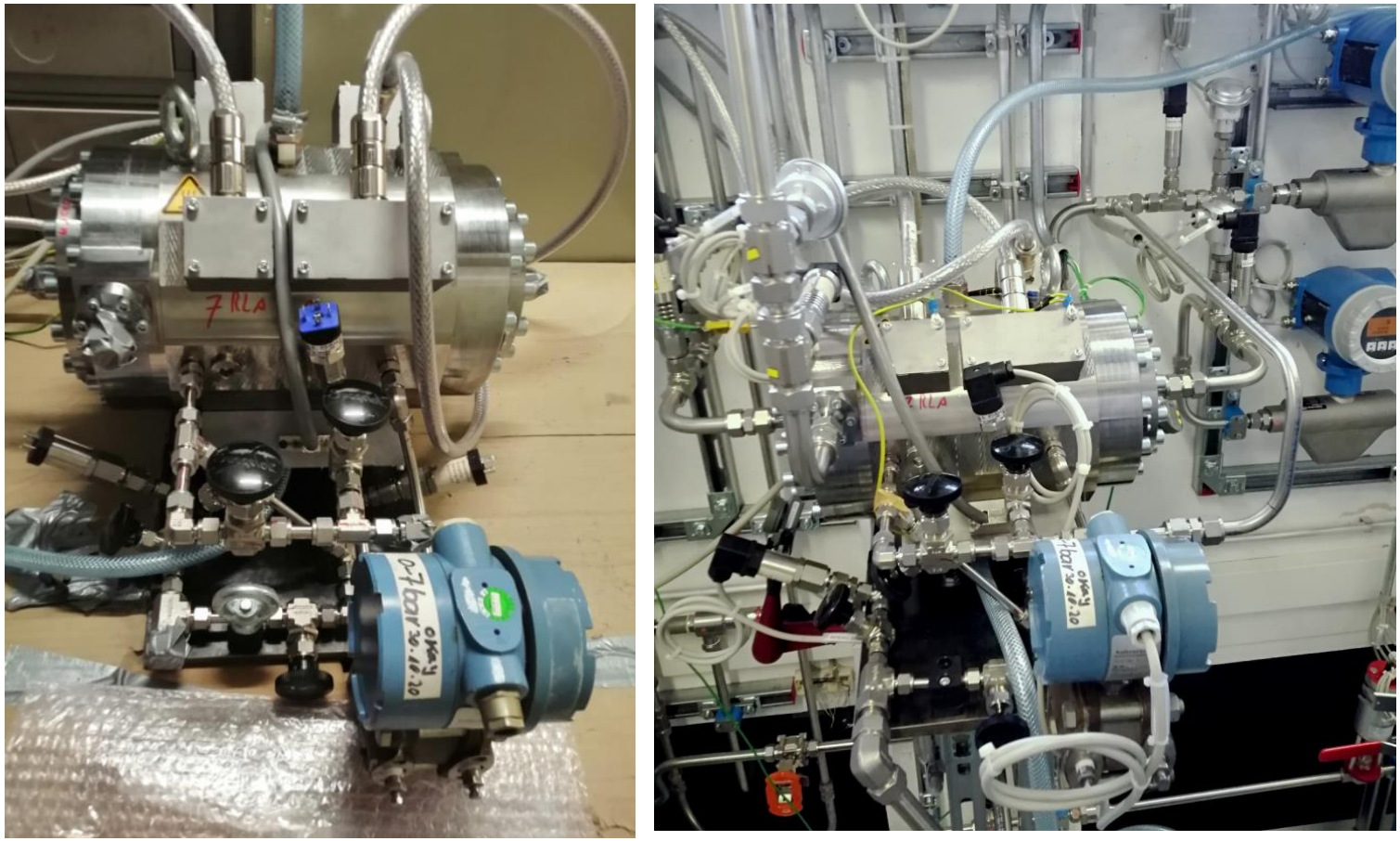

Figure 13: Improved TAC fully assembled during commissioning tests with air (left) and integrated in the sCO2-HeRo cycle (right)